Phase Transformation Behavior of Medium Manganese Steels with 3 Wt Pct Aluminum and 3 Wt Pct Silicon During Intercritical Annealing

BINHAN SUN, FATEH FAZELI, COLIN SCOTT, and STEPHEN YUE

Medium manganese steels alloyed with sufficient aluminum and silicon amounts contain high fractions of retained austenite adjustable to various transformation-induced plasticity/twinning-induced plasticity effects, in addition to a reduced density suitable for lightweight vehicle body-in-white assemblies. Two hot rolled medium manganese steels containing 3 wt pct aluminum and 3 wt pct silicon were subjected to different annealing treatments in the present study. The evolution of the microstructure in terms of austenite transformation upon reheating and the subsequent austenite decomposition during quenching was investigated. Manganese content of the steels prevailed the microstructural response. The microstructure of the leaner alloy with 7 wt pct Mn (7Mn) was substantially influenced by the annealing temperature, including the variation of phase constituents, the morphology and composition of intercritical austenite, the M_s temperature and the retained austenite fraction. In contrast, the richer variant 10 wt pct Mn steel (10Mn) exhibited a substantially stable ferrite-austenite duplex phase microstructure containing a fixed amount of retained austenite which was found to be independent of the variations of intercritical annealing temperature. Austenite formation from hot band ferrite-pearlite/bainite mixtures was very rapid during annealing at 1273 K (1000 °C), regardless of Mn contents. Austenite growth was believed to be controlled at early stages by carbon diffusion following pearlite/bainite dissolution. The redistribution of Mn in ferrite and particularly in austenite at later stages was too subtle to result in a measureable change in austenite fraction. Further, the hot band microstructure of both steels contained a large fraction of coarse-grained δ-ferrite, which remained almost unchanged during intercritical annealing. A recently developed thermodynamic database was evaluated using the experimental data. The new database achieved a better agreement with the experimental results for the 7Mn steel compared with the existing commercial TCFE database; however, some discrepancy in the predicted phase fractions and compositions still existed. The phase transformation behavior of the two steels during annealing and its implication on the design of high aluminum-silicon medium manganese steels were discussed in detail.

I. INTRODUCTION

ROAD transportation vehicles are required to meet stringent standards on fuel economy, emissions and safety by 2025. Vehicle manufacturers are currently developing new lightweight body-in-white assemblies with intensive use of advanced high strength steels (AHSS) to ensure crashworthiness and rigidity. To this end, substantial research and development activities are proceeding globally to deploy superior AHSS grades, so-called third generation AHSS (3rd Gen), with target performance exceeding the properties of conventional dual phase (DP) and transformation-induced plasticity (TRIP) steels. One of the strong candidates for 3rd Gen AHSS is medium Mn steels containing nearly 3 to 10 wt pct Mn.[1–3] High volume fraction of retained austenite (up to 70 vol pct) stabilized by the increased Mn contents constitutes a key advantage of this class of 3rd Gen AHSS and offers excellent mechanical performance.[2,4–10] In particular, the required processing route is relatively simple and consists of a controlled intercritical annealing (IA) treatment without a need for subsequent bainite overaging or martensite quenching-partitioning.[8,11,12] However, numerous microstructures containing different combinations of ferrite, austenite, and martensite/bainite with various phase fractions can be produced depending on the IA parameters.[5,8,13] Further, partitioning of C and substitutional alloying elements during annealing alters the response of the retained austenite upon subsequent forming operations or in-service deformations.[8,12,14–16] As such, it is crucial to explore and understand the microstructural evolution during intercritical annealing of medium Mn

BINHAN SUN, Graduate Student, and STEPHEN YUE, Professor, are with the Department of Materials Engineering, McGill University, 3610 University St. Montreal QC, H3A 0C5, Canada. Contact e-mail: binhan.sun@mail.mcgill.ca FATEH FAZELI and COLIN SCOTT, Research Scientists, are with CanmetMATERIALS, Natural Resources Canada, 183 Longwood Rd S, Hamilton ON, L8P 0A5, Canada.

steels with the main target to define optimized processing parameters for increased fraction and stability of the retained austenite in the final 3rd Gen AHSS sheet or strip products.

Recently, several medium Mn steels alloyed with relatively high Al and/or Si contents have attracted considerable attentions. The total content of Al and Si is typically higher than ~4 wt pct in these alloys,[5,15–20] leading to a reduced overall density.[21] In particular, the stacking fault energy (SFE) of austenite can be tailored by Al and Si additions to promote various TRIP/TWIP effects, giving rise to a further improvement of mechanical property.[15,16,18–20,22–24] For example, our previous study found that both TRIP and TWIP effect could be activated to achieve a noticeable combination of strength-ductility balance of 27,000 MPa pct in a hot rolled 10Mn-3Al-3Si alloy.[5,22] However, high amounts of Al and Si in these steels stabilize ferrite and enlarge the two-phase ($\alpha + \gamma$) domain so that thermomechanical processing in the two-phase range cannot be avoided.[17] The ensuing hot/cold rolled microstructure is often complicated containing a certain amount of δ-ferrite along with retained austenite and other phases.[19,25–27] To the best of our knowledge, there are no detailed literature reports on the evolution and response of this complex microstructure upon subsequent intercritical processing. Further, accurate thermodynamic data for this group of medium Mn steels are unavailable currently, which constitutes extra challenges to preselect suitable annealing parameters.

The scope of the present study was the microstructural evolution of 7 and 10 wt pct medium Mn hot rolled steels containing 3 wt pct Al and Si upon different intercritical annealing treatments, with the main objective to provide a better understanding on the microstructural control for this type of medium Mn steels. The work focused on hot rolled products, which share similar features with cold rolled sheets in terms of intercritical austenite formation and alloy partitioning. As such, the ensuing insights especially the effect of annealing parameters on fraction, composition and stability of retained austenite can be readily exploited for processing of cold rolled high Si-Al, medium Mn 3rd Gen AHSS sheets. Further, considering the lack of accurate thermodynamic description for these high Al-Si medium Mn steels, the current results are deemed very beneficial for development of more reliable thermodynamic database for similar steels. The assessment of microstructure-property correlations of the studied steels is the subject of ongoing study and is not presented here.

II. EXPERIMENTAL PROCEDURE

The chemical compositions of the medium Mn steels are shown in Table I, and herein they are referred to as 7Mn and 10Mn. The steel melts were prepared in a vacuum induction furnace and cast into 100 kg ingots. Following homogenization at 1473 K (1200 °C) for 3 hours, the ingots were hot rolled in the temperature range from 1373 K to 1023 K (1100 °C to 750 °C) and air cooled. The coiling process was then simulated by maintaining the hot bands at ~873 K (600 °C) and furnace cooling.

Specimens were cut from the hot rolled plates and subjected to heat treatments in a box furnace with a protective argon atmosphere, followed by water quenching. A secondary thermocouple was positioned in contact with the samples to ensure a precise control of the temperature. The effect of annealing temperature and time on microstructural evolution was investigated separately. The first set of samples was annealed at various temperatures ranging from 973 K to 1473 K (700 °C to 1200 °C) with 100 K increments for 1 hour. The second set was subjected to a constant temperature of 1273 K (1000 °C) for different holding times between 1 minute and 5 hour.

Microstructure observations were performed with a Nikon Epiphot 200 optical microscope (OM) and a Hitachi SU3500 scanning electron microscope (SEM) equipped with an electron backscattered diffraction (EBSD) detector. Samples for OM and SEM examinations were etched with 2 pct nital followed by 10 pct aqueous sodium metabisulfite ($Na_2S_2O_5$). For EBSD observation, samples were finally polished with 0.05 μm colloidal silica for 4 to 8 hours in a vibratory polisher. The austenite fraction of the samples was determined by X-ray diffraction (XRD) using Co K_α radiation, operated at 35 kV and 45 mA with scan step size of 0.02 deg. The acquired data were analyzed by the Reitveld whole diffraction pattern fitting procedures[28] implemented by the TOPAS 4 software. The pearlite, bainite, and martensite volume fractions were measured based on the ASTM E1245-03 standard,[29] using the image processing software ImageJ; more than 15 OM micrographs taken in a relatively low magnification (200 times) were randomly selected for this measurement. Austenite grain size was determined by the standard linear intercept method[30] based on the OM and SEM images; about 200 intercepts were yielded for each measurement for a standard deviation of less than 20 pct.

Composition analysis (Mn, Al, and Si) for specific phases was performed in SEM using Energy-Dispersive X-ray Spectrometer (EDS). The average C content of austenite was determined from the XRD data by adopting the equation proposed by Dyson and Holmes:[31,32]

$$a_\gamma(\text{Å}) = 3.556 + 0.0453x_C + 0.00095x_{Mn} + 0.0056x_{Al},$$

where α_γ is austenite lattice parameter, x_C, x_{Mn}, and x_{Al} are concentrations of C, Mn, and Al in austenite (wt pct), respectively. In the present study, α_γ was determined from the interplanar spacing (d_{hkl}) of the (111) peak of austenite,[33] which is the most pronounced peak in the XRD pattern and should yield the highest accuracy. The phase composition measurements by EDS/XRD were conducted for different randomly selected locations of each specimen, and the values were averaged. It should be noted that all the error bars shown in this paper reflect the relative deviation from several measurements for different sample locations; the precision of the techniques was not included.

Table I. Steel Compositions in Weight Percent

Alloy	C	Mn	Al	Si	Mo	Fe
7Mn	0.22	7.15	3.11	3.21	0.05	balance
10Mn	0.20	10.02	3.17	3.19	0.06	balance

III. RESULTS

A. Hot Rolled Microstructure

Figure 1 shows the hot band microstructures of the 7Mn and 10Mn steel illustrating elongated bands due to hot rolling in two-phase region. In the 7Mn steel (Figures 1(a) and (b)), three different phases are identified: δ-ferrite (δ), pearlite (P), and bainite (B). Pearlite in conjunction with bainite transformed from the prior austenite during the coiling simulation process. The volume fractions of pearlite and bainite in the hot rolled 7Mn steel are 32.2 ± 1.5 pct and 8.2 ± 0.7 pct, respectively, measured by the image analysis using OM micrographs. Retained austenite was not found in the hot rolled microstructure of the 7Mn steel, as also confirmed by XRD measurements (Figure 1(d)). In contrast for the 10Mn steel, a large amount of retained austenite (γ) exists (37.9 ± 2.7 vol pct measured by XRD) in the microstructure of the hot bands. Only a small amount of pearlite (7.4 ± 0.6 vol pct measured by OM image analysis) is present on the edge of the austenite islands.

B. Effect of Annealing Temperature

The microstructure of the 7Mn steel is highly influenced by the reheating temperature during subsequent annealing of the hot bands. As shown in Figure 2, the initial pearlite and bainite transform completely to austenite and ferrite after 1 hour annealing at 1073 K (800 °C). However, the banded features of the hot rolled microstructure remain unchanged, consisting of contiguous δ-ferrite regions engulfing austenite/ferrite bands. EBSD and SEM images show that both intercritical austenite (γ) and ferrite (α) adopt two distinct morphologies: lath shape and globular shape annotated by elliptical and rectangular frames, respectively in Figures 2(a) and (b) and labeled by γ_G, γ_L, α_G and α_L. It was confirmed in the previous work[27] that the globular-shaped phases were transformed from pearlite, whereas the austenite and ferrite formed from bainite have the lath morphology. It seems that γ_L nucleates from the fine lath-like carbide particles in the initial bainite, as also reported by Huang[11] who studied a 0.1C-5Mn steel with an initial bainite plus martensite microstructure. The grain size of γ and α is fine, *i.e.*, ~2.5 μm for globular-shaped phases and less than 1 μm in width for lath-shaped phases, whereas the δ-ferrite grains are coarse (50 to 100 μm). The Mn content of γ_L is 8.7 ± 0.2 wt pct, which is lower than that of γ_G (9.6 ± 0.1 wt pct). Conversely, α_L has a higher Mn concentration (6.8 ± 0.2 wt pct) than α_G (6.1 ± 0.2 wt pct). When the 7Mn hot rolled specimen is subjected to a heat treatment at 1273 K (1000 °C), some portion of

austenite grains transforms to martensite upon quenching, giving rise to a multi-phase microstructure of ferrite, martensite plus retained austenite (FMNA), as illustrated by Figure 3. The α'-martensite with the BCT crystal structure in Figure 3 was identified by its higher dislocation density which yields a higher local misorientation value.[34] Lath-shaped morphology was no longer observed for this scenario, which could be due to recrystallization or most likely coarsening driven by the decrease in the total surface energy.

Figure 4 shows the microstructure of the 10Mn steel after annealing at 1073 K (800 °C) for 1 hour. The initial austenite and δ-ferrite aggregate bands remained intact during annealing. A small amount of newly formed austenite (γ_{NT}) and ferrite with a globular shape has transformed from the pearlite in the hot rolled microstructure, as seen more clearly in Figure 4(c). The grain size of the globular austenite and ferrite was estimated to be ~2 μm. EDS measurement revealed that γ_{NT} had a higher Mn content (14.2 ± 0.2 wt pct) than the initial γ austenite (11.4 ± 0.1 wt pct), whereas α had a lower Mn content (8.9 ± 0.3 wt pct) than the δ-ferrite (9.5 ± 0.1 wt pct). At a higher annealing temperature of 1273 K (1000 °C), the γ_{NT} tends to merge with the initial austenite and cannot be differentiated, leading to a smoother edge of the austenite bands (Figure 5). Further, the small α-ferrite grains seem to have lower volume fraction and larger grain size (~4 μm), probably due to some coarsening. Nonetheless, it is obvious that the microstructure of the 10Mn steel is not very sensitive to the annealing temperature.

For both alloys, the EBSD results (Figures 2 through 5) indicate that at the higher annealing temperature, 1273 K (1000 °C), δ-ferrite exhibits a wider range of crystallographic orientations and a finer grain size. This may be attributed to the enhanced recrystallization of δ-ferrite grains at higher annealing temperatures. It is likely that dynamic recrystallization in both phases during hot rolling was not completed, and the microstructure still remained somewhat deformed after subsequent cooling. The complex response of the ferrite-austenite mixture to different hot deformation temperatures and respective restoration scenarios for the 10Mn alloy have been studied in detail elsewhere.[17] Table II compares the recrystallized fraction of each phase in the 10Mn steel after annealing at different temperatures and subsequent quenching. In general, more austenite and ferrite recrystallized at the higher annealing temperature. It is also interesting to note that ferrite has a higher recrystallized fraction than austenite at both annealing temperatures, which is related to the different recrystallization kinetics of the two phases.[17]

The phase fractions of the 7Mn and 10Mn steels under different annealing temperatures and subsequent
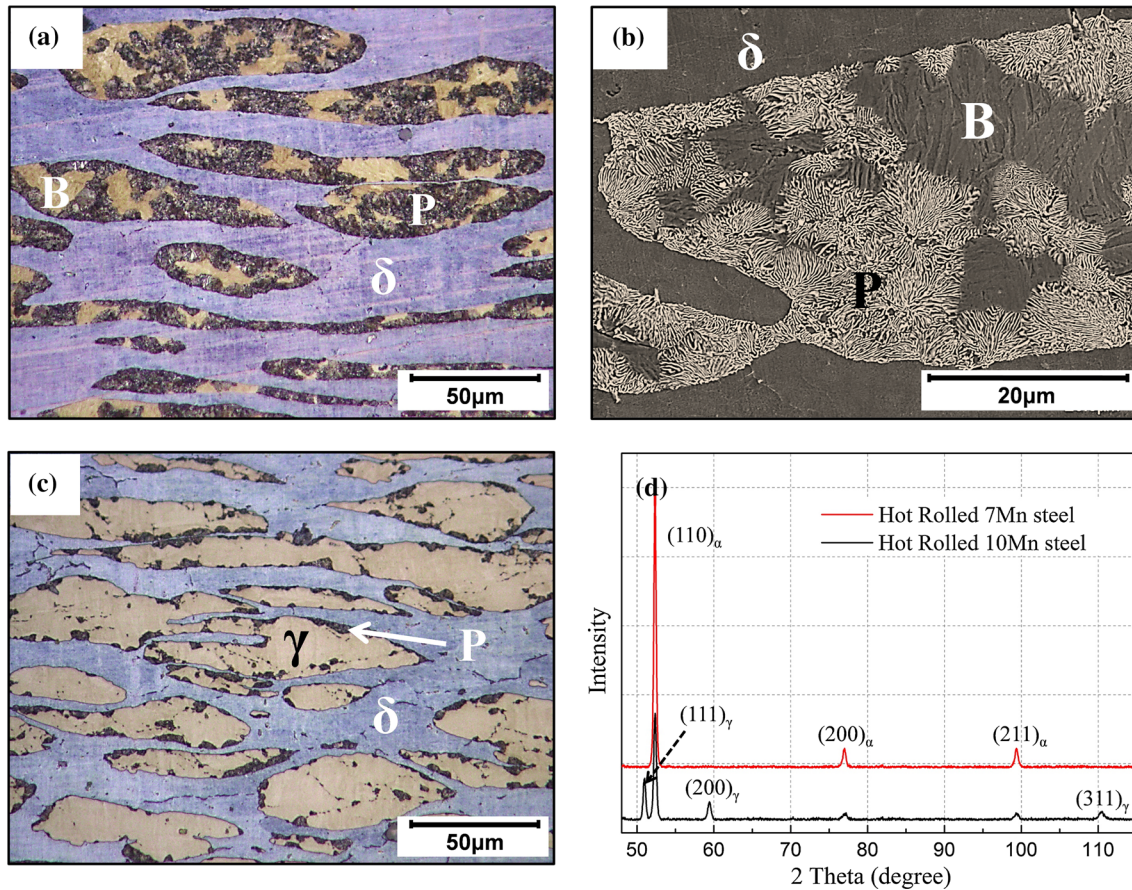
Fig. 1—(a) Optical and (b) SEM micrographs of the hot rolled structure of the 7Mn steel; (c) Optical micrograph of the hot rolled 10Mn steel; (d) XRD patterns of the hot band microstructures (P: Pearlite; B: Bainite; γ: Austenite; δ: δ-ferrite, samples were etched by 2 pct nital followed by 10 pct aqueous sodium metabisulfite).

quenching are shown in Figure 6. For both steels, microstructural characterization reveals that the onset of austenite formation occurs above 973 K (700 °C). The 7Mn steel (Figure 6(a)) shows a ferrite-austenite duplex phase (FADP) microstructure at 1073 K and 1173 K (800 °C and 900 °C), whereas the FMNA microstructure was observed for higher annealing temperatures. The martensite fraction increases with increasing annealing temperature above 1273 K (1000 °C), which results in a lower fraction of retained austenite. Any diffusional phase transformation during water quench was unlikely to occur due to very fast cooling rate, i.e., ~85 K/s. Therefore, the fraction of initial austenite at annealing temperatures can be estimated simply by the combined volume fractions of retained austenite and martensite at room temperature. The result was plotted as a blue dashed line in Figure 6(a). It appears that the volume fraction of initial austenite prior to cooling increases rapidly from 973 K to 1173 K (700 °C to 900 °C) and then stabilizes with a very slight decrease at 1473 K (1200 °C) in the 7Mn steel. However for the 10Mn steel, only the FADP microstructure was observed after quenching from annealing temperatures above 1073 K (800 °C) (Figure 6(b)). The findings imply that initial austenite in the 10Mn steel is sufficiently stable to resist subsequent decomposition during cooling. The austenite

fraction in the 10Mn steel first increases with increasing temperature to 1073 K (800 °C), stabilizes, and slightly decreases at 1473 K (1200 °C). It was also found that the 10Mn steel had around 10 vol pct more austenite than the 7Mn steel at temperatures higher than 1073 K (800 °C) prior to quenching, which indicates the significant role of Mn on stabilizing austenite.

The experimental average solute contents of the intercritical austenite with annealing temperature are illustrated in Figure 7. The thermodynamic calculation for the austenite composition was also plotted together and the comparison will be discussed in "Section IV." As mentioned above, the austenite composition (Mn, Al, and Si) of the 7Mn steel also depends on its morphology, i.e., lath shape and globular shape, which is transformed from prior bainite and pearlite, respectively. The volume fractions of γ_L and γ_G could be estimated, based on an assumption that the volume fraction ratio of γ_L to γ_G in the annealed samples equals the fraction ratio of prior bainite to pearlite (8.2/32.2). Therefore, the average austenite Mn, Al, and Si contents shown in Figure 7(a) were calculated by the following equation:

$$w_i(\gamma, \text{average}) = [w_i(\gamma_L) \times f(\gamma_L) + w_i(\gamma_G) \times f(\gamma_G)]/f(\gamma) \quad [1]$$
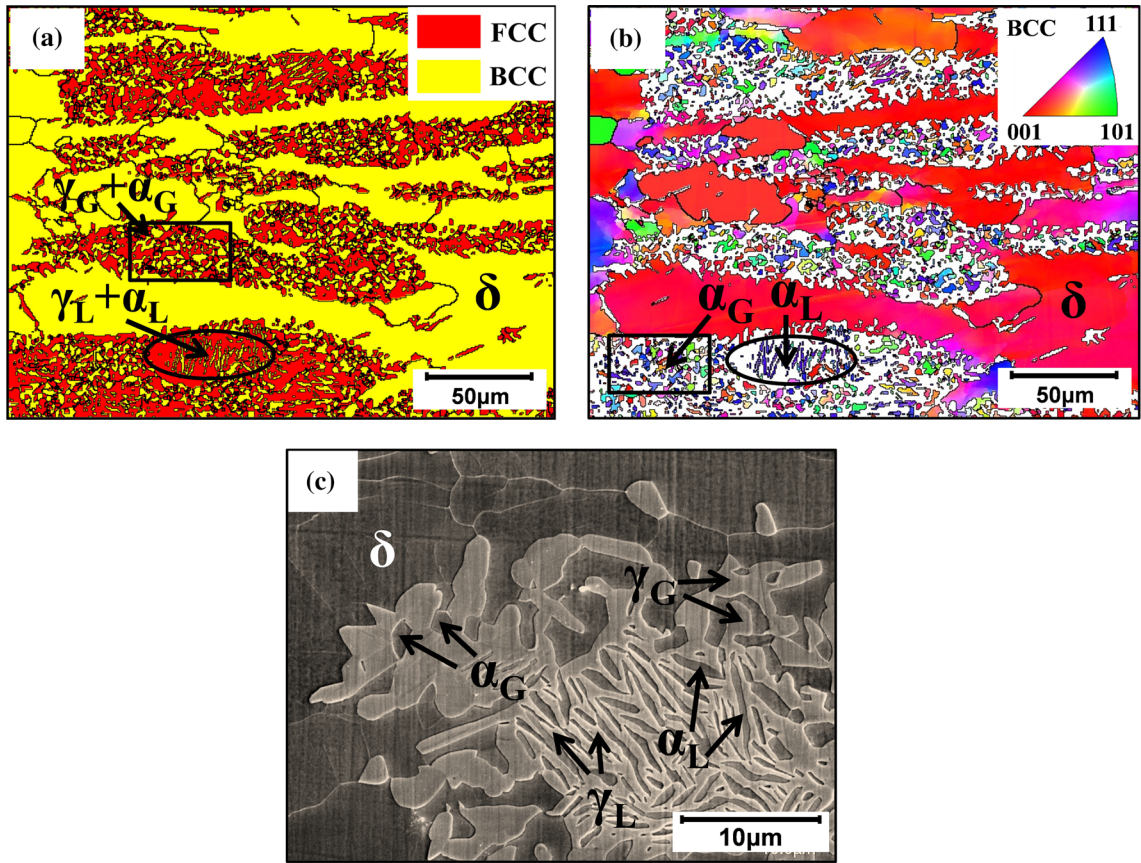
Fig. 2—Microstructure of the 7Mn steel annealed at 1073 K (800 °C) for 1 h: (a) EBSD phase mapping showing FCC and BCC phases; (b) BCC inverse pole figure (IPF) in the same area of (a); (c) SEM micrograph in the higher magnification, etched by 2 pct nital followed by 10 pct aqueous sodium metabisulfite (γ_G: globular-shaped austenite; γ_L: lath-shaped austenite; α_G: globular-shaped ferrite; α_L: lath-shaped ferrite).
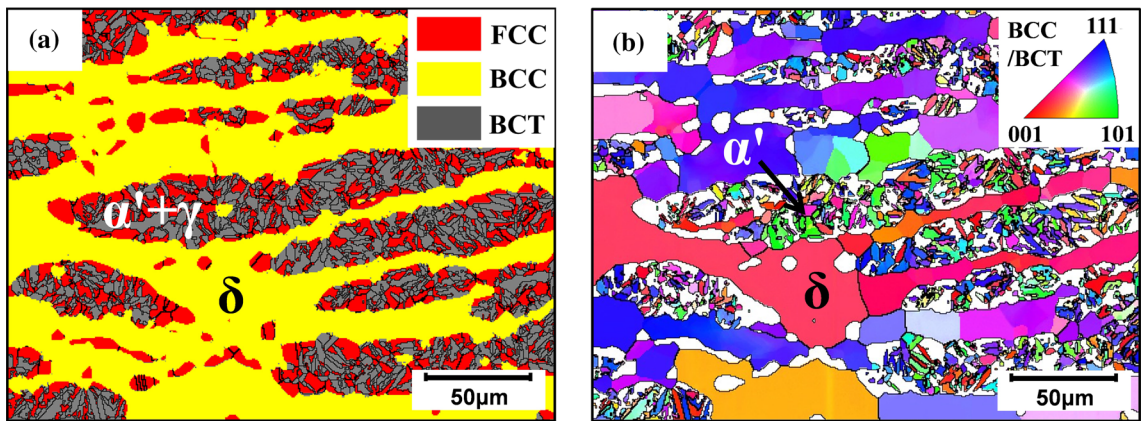
Fig. 3—EBSD images of the 7Mn steel annealed at 1273 K (1000 °C) for 1 h: (a) Phase mapping showing FCC, BCC and BCT phases; (b) BCC/BCT inverse pole figure in the same area of (a).

where w_i is the contents of Mn, Al, or Si (in wt pct), $f(\gamma_L)$ and $f(\gamma_G)$ are the volume fraction of the lath-shaped austenite and globular-shaped austenite, respectively. However, the lath-shaped phases in the 7Mn steel disappeared when the annealing temperature is above 1173 K (900 °C); therefore, only the composition of γ_G was taken into account at these conditions. In addition, although the newly transformed austenite (γ_{NT}) appeared in the 10Mn steel also possesses a slight

different composition, it can only be observed in the samples annealed at 1073 K (800 °C) and the fraction is quite small, therefore, the composition values in γ_{NT} were not counted in Figure 7(b). For the 7Mn steel, as shown in Figure 7(a), Mn, Al, and Si contents show a monotonic trend with temperature; a decrease of Mn and a slight increase of Al and Si. Carbon concentration first decreases from 1073 K to 1373 K (800 °C to 1100 °C) and then slightly increases at higher temperatures.
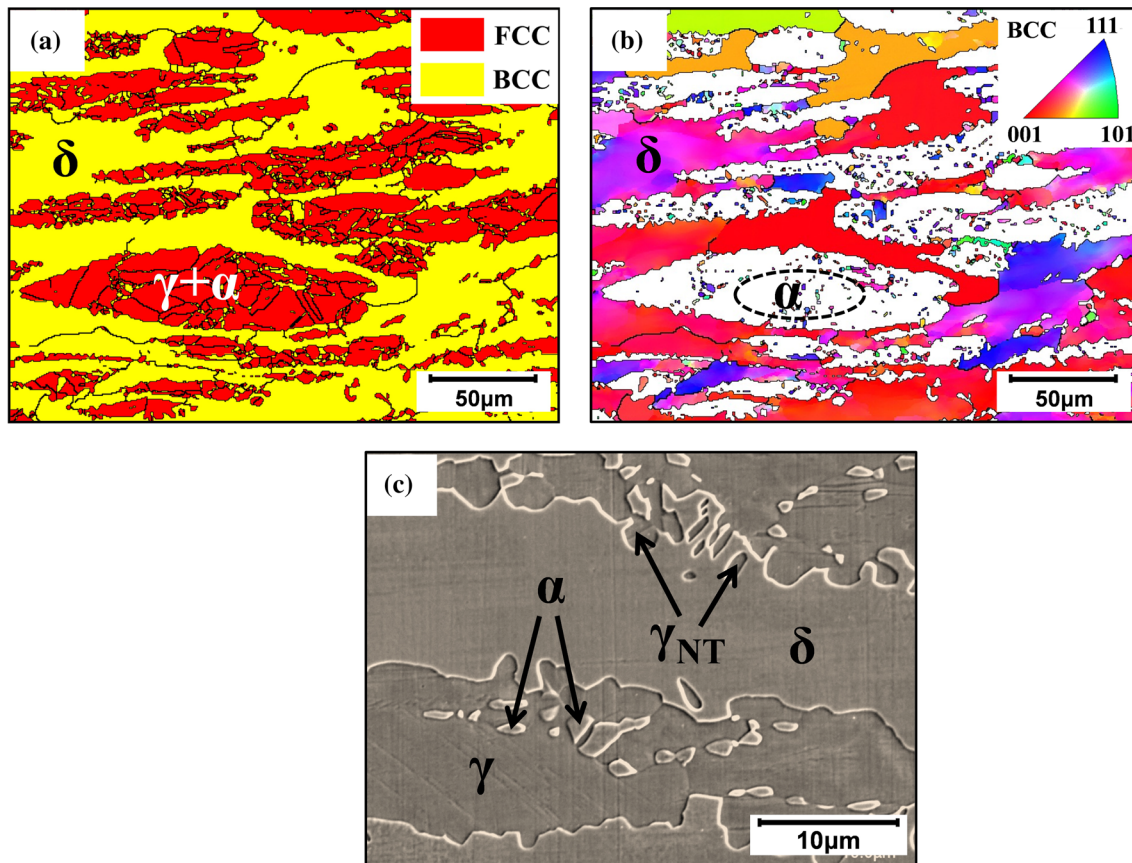
Fig. 4—Microstructure of the 10Mn steel heat treated at 1073 K (800 °C) for 1 h: (a) EBSD phase mapping showing FCC and BCC phases; (b) BCC inverse pole figure in the same area of (a); (c) SEM micrograph in the higher magnification, etched by 2 pct nital followed by 10 pct aqueous sodium metabisulfite (γ_{NT}: newly transformed austenite).
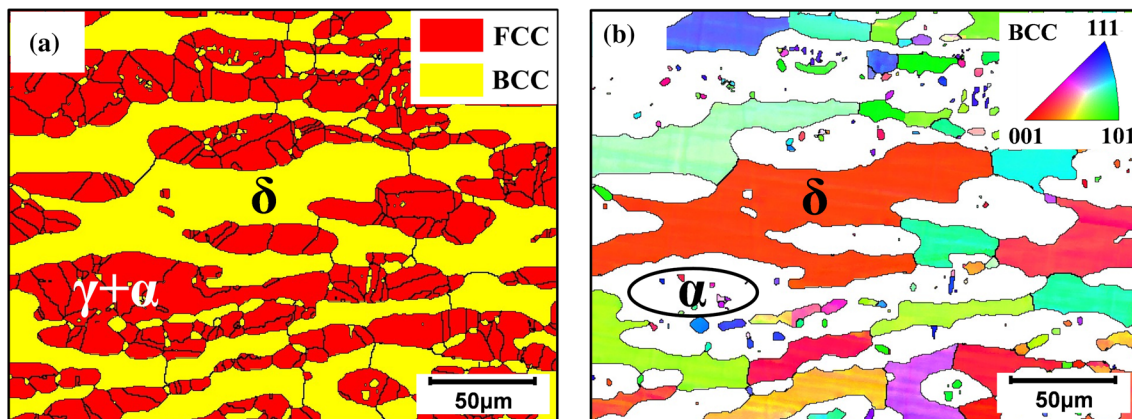

Fig. 5—EBSD images of the 10Mn steel heat treated at 1273 K (1000 °C) for 1 h: (a) Phase mapping showing FCC and BCC phases; (b) BCC inverse pole figure in the same area of (a).

Table II. Recrystallized Fractions (Vol Pct) of Austenite and Ferrite in the 10Mn Steel After Annealing at Different Temperatures and Subsequent Quenching (Measured by EBSD)

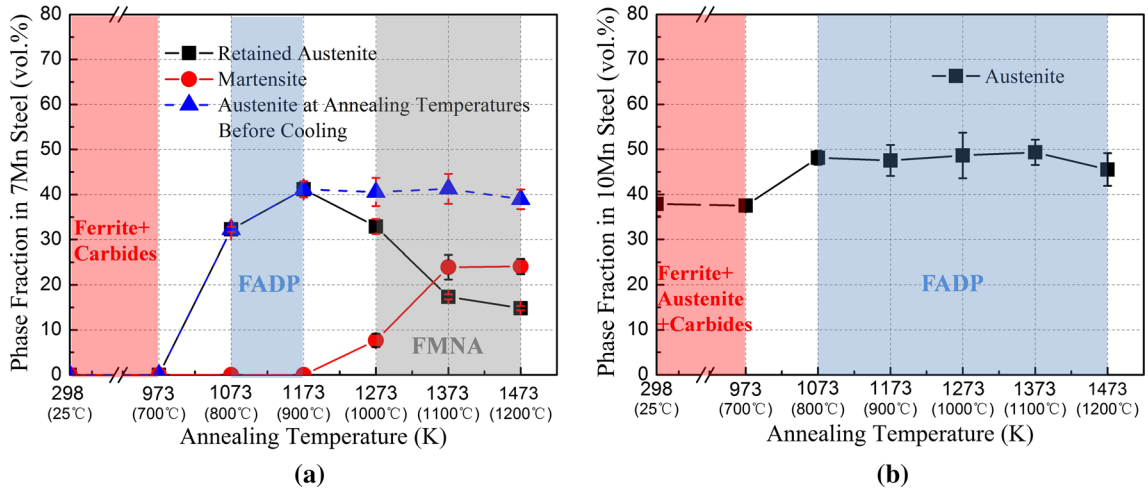| Austenite Phase	1073 K (800 °C)	1273 K (1000 °C)	Ferrite Phase	1073 K (800 °C)	1273 K (1000 °C)
Recrystallized	9.85	42.1	Recrystallized	38.65	71.15
Substructured	50.2	56.85	Substructured	57.25	27.5
Deformed	39.95	1.05	Deformed	4.1	1.35

Fig. 6—Phase fractions of (a) the 7Mn steel and (b) the 10Mn steel under different annealing temperatures and subsequent quenching (FMNA: ferrite, martensite plus retained austenite microstructure; FADP: ferrite-austenite duplex phase microstructure).
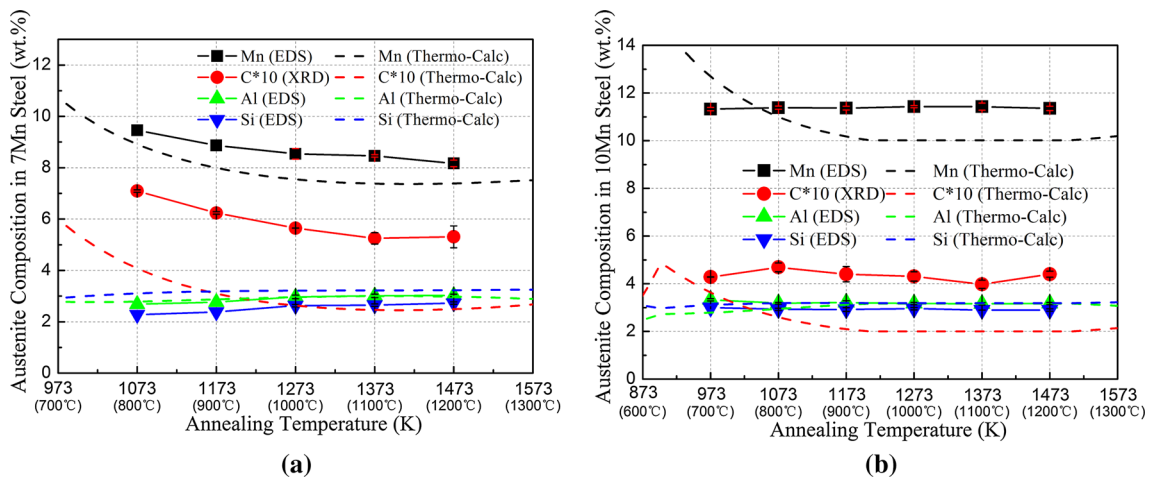

Fig. 7—Calculated equilibrium and measured average solute (C, Mn, Al, and Si) contents of the intercritical austenite in (a) the 7Mn steel and (b) the 10Mn steel as a function of annealing temperature (the thermodynamic calculation was conducted using Thermo-Calc software with a modified database).

However, regarding the 10Mn steel (Figure 7(b)), Mn, Al, and Si contents of the intercritical austenite remain unchanged at different annealing temperatures. The C concentration of the austenite increases initially from 973 K to 1073 K (700 °C to 800 °C), presumably due to carbides dissolution in austenite at 1073 K (800 °C). Subsequently, a decrease of C content is observed up to 1373 K (1100 °C), followed by an increase at 1473 K (1200 °C). It is noticed that the annealing temperature has a more pronounced influence on the austenite composition of the 7Mn steel.

The martensite start (M_s) temperature of the inter-critical austenite at different annealing temperatures was calculated for the two steels. The following empirical equation accounting for composition and grain size effect was selected:[35]

$$M_s(°C) = 545 - 423w_C - 30.4w_{Mn} - 60.5V_\gamma^{-1/3} \quad [2]$$

where w_C and w_{Mn} are the C and Mn contents of the austenite (in wt pct); the experimental values in

Figure 7 were used in the calculation, and V_γ is the effective grain volume of the austenite (in μm^3). The Koistenen–Marburger (KM) empirical equation[36] was adopted to estimate the fraction of martensite:

$$f_M = \left\{ 1 - \exp\left[-\alpha \left(M_s - T_q \right)^\beta \right] \right\} \times f_\gamma \quad [3]$$

where f_M is the martensite fraction transformed from austenite, f_γ is the austenite fraction under annealing temperatures before cooling, T_q is the quenching temperature (here 298 K (25 °C)), and α and β are constants[37]: $\alpha = 0.0231 - 0.0105w_C$; $\beta = 1.4304 - 1.1836w_C + 0.7527w_C^2$.

Figure 8(a) illustrates the calculated M_s temperature of the 7Mn and 10Mn steels at different annealing temperatures, without austenite grain size consideration. For the 7Mn steel, it shows that the M_s temperature increases with annealing temperature. The M_s temperature of the 7Mn steel remains above room temperature, 298 K (25 °C), for annealing temperatures higher than 1273 K (1000 °C), which could explain the transition of
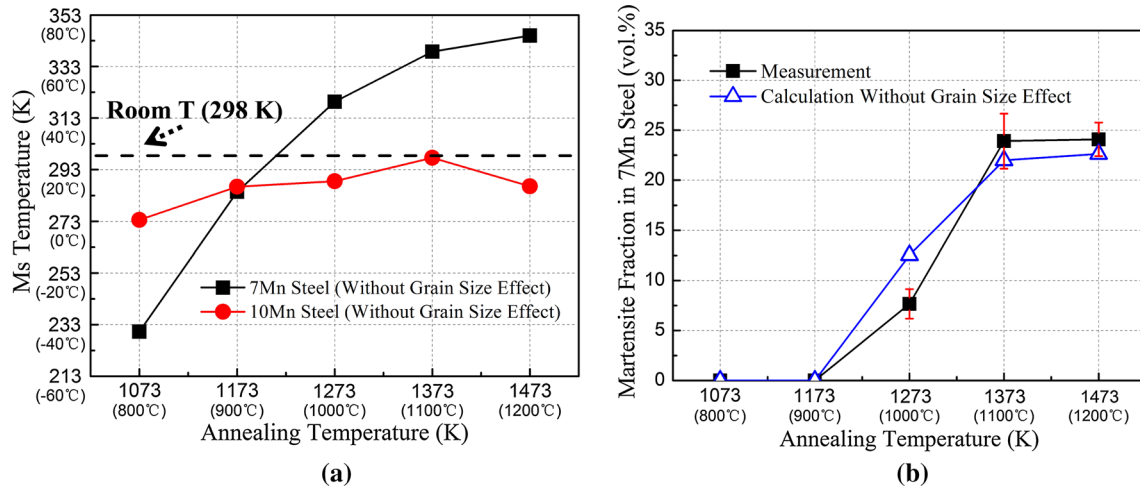
Fig. 8—(a) Calculated M_s temperature of the 7Mn and 10Mn steels as a function of annealing temperature; (b) Martensite fraction of the 7Mn steel at different annealing temperatures.
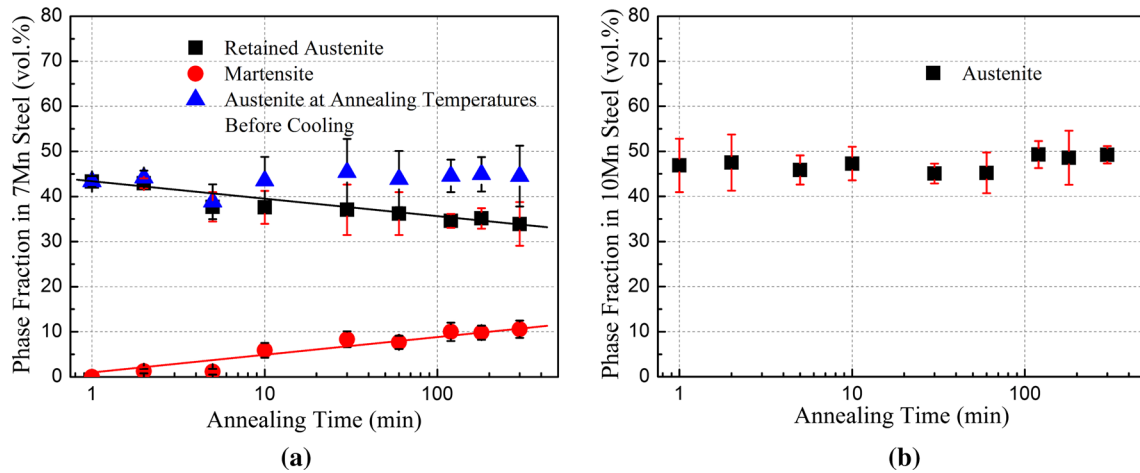

Fig. 9—Phase fractions of (a) the 7Mn steel and (b) the 10Mn steel as a function of annealing time at 1273 K (1000 °C).

FADP to FMNA microstructure at higher annealing temperatures for the 7Mn steel. The calculated martensite fraction in the 7Mn steel adopting KM equation is shown in Figure 8(b); a good agreement between the calculation and measurement can be found. Martensite in the 7Mn steel increases rapidly from 1173 K to 1373 K (900 °C to 1100 °C) and approaches a plateau at higher temperatures. However, although the austenite in the 10Mn steel contains slightly less C than that in the austenite of the 7Mn steel (Figure 7), the higher Mn content of the 10Mn steel maintains the M_s temperature below room temperature for all the examined annealing temperatures. Therefore, only the FADP microstructure can be obtained in the 10Mn steel.

C. Effect of Annealing Time

Different annealing times were conducted at 1273 K (1000 °C), followed by water quenching to study the kinetics of phase transformation in the two medium Mn steels.

Figure 9 shows the volume fractions of different phases as a function of annealing time at 1273 K (1000 °C) for the two medium Mn steels. Austenite transformation is very rapid in both steels, e.g., nearly 40 vol pct austenite has been transformed in the 7Mn steel after only 1 minute holding (the microstructures can be found elsewhere[27]). In the 7Mn steel, as shown in Figure 9(a), the retained austenite fraction is the highest after annealing for 1 min, and martensite starts to form after 2 minutes and increases with time continuously, consuming some of the retained austenite. However, the austenite fraction before quenching in the 7Mn steel is almost constant after 1 minute. For the 10Mn steels (Figure 9(b)), martensite was never observed under any condition. The initial austenite fraction is 37.9 ± 2.7 vol pct in the hot rolled microstructure. After 1-minute annealing, it increases to 46.9 ± 5.9 vol pct; however, with increasing annealing time, the austenite fraction changes slightly (45 to 49 vol pct) without a clear trend with holding time.
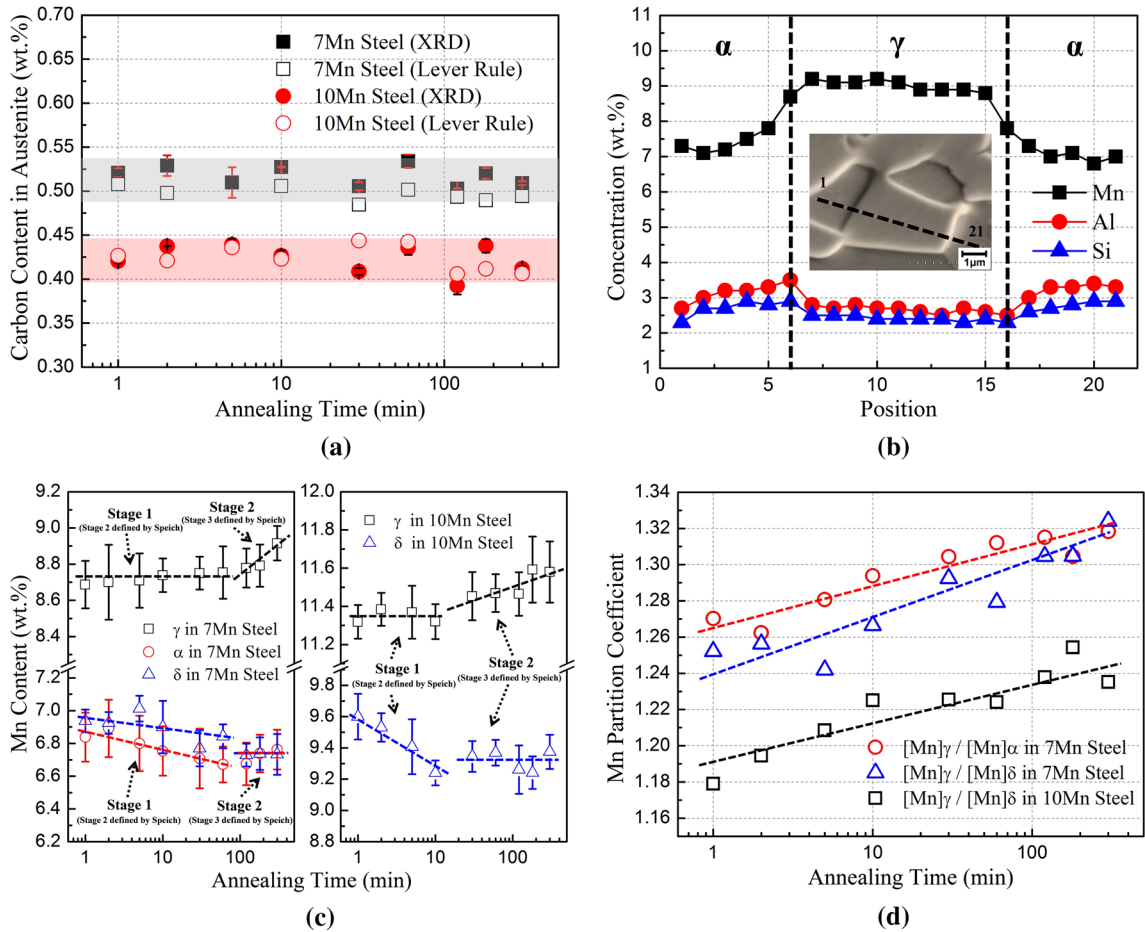
Fig. 10—(a) Measured and calculated C contents in the austenite phase of the two medium Mn steels as a function of holding time at 1273 K (1000 °C); (b) The distribution of Mn, Al, and Si across an austenite island in the 7Mn steel annealed at 1273 K (1000 °C) for 1 min; (c) Manganese contents with annealing time in austenite and ferrite of both steels; (d) Manganese partition coefficients between austenite and ferrite in both steels.
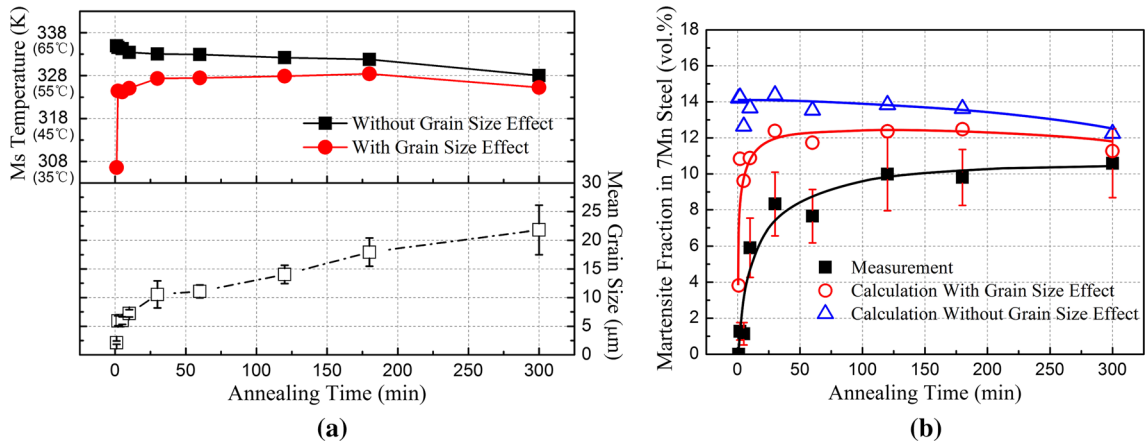

Fig. 11—(a) Austenite grain size and calculated M_s temperature of the 7Mn steel as a function of annealing time; (b) Martensite fraction of the 7Mn steel at different annealing times.

The austenite C contents measured by XRD in the two medium Mn steels annealed for different times at 1273 K (1000 °C) are shown in Figure 10(a). The figure also plotted the calculated values based on the lever rule under the assumption that C was not soluble in ferrite; a strong match is observed between the measured and calculated values. There is no clear relationship between austenite C concentration and
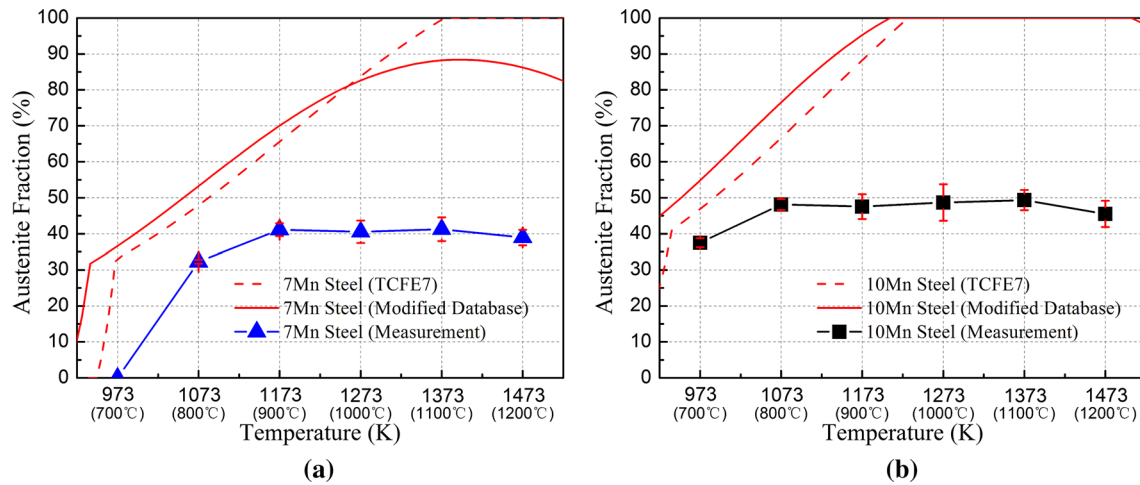
Fig. 12—Comparison of the austenite fraction between thermodynamic predictions and experimental measurement in (a) the 7Mn steel and (b) the 10Mn steel.

annealing time for both grades. Additionally, both measured and calculated C concentrations show some scatter, which is believed to stem from several error sources (e.g. XRD measurements and Dyson's equation). Solute partitioning occurs during intercritical annealing, as reported by several researchers.[12,14,15,38] Figure 10(b) gives the distribution of Mn, Al, and Si across a fine intercritical austenite island in the 7Mn steel annealed at 1273 K (1000 °C) for 1 minute. It shows that austenite is enriched by Mn but depleted with respect to Al and Si after annealing, even for a short 1-minute holding. Figure 10(c) plots the Mn contents in austenite and ferrite of the two steels, and the Mn partition coefficients between austenite and ferrite were calculated and are shown in Figure 10(d). For both steels, Mn concentration is increasing in austenite and reducing in ferrite in the global trend during annealing (Figure 10(c)), resulting in a more pronounced Mn partitioning between austenite and ferrite, illustrated in Figure 10(d). However, the change of Mn content in the two phases of both steels can be divided into two stages: in stage 1, Mn keeps depleting in ferrite while remaining stabile, or slightly increasing, in austenite; then the Mn content maintains an almost constant level in ferrite while increases in austenite, which characterizes stage 2 in Figure 10(c). This separate Mn diffusion stages will be discussed in "Section IV." It is also interesting to note that intercritical ferrite (α) in the 7Mn steel has a lower Mn concentration than δ-ferrite (leading to a higher Mn partition coefficient); however, these two curves almost converge at longer annealing times. It is illustrated by Figure 10(d) that the 7Mn steel has higher Mn partition coefficients than the 10Mn steel.

The calculated M_s temperature and martensite fraction for the 7Mn steel at different annealing times are illustrated in Figure 11. Accounting for compositional effect, the M_s temperature maintains almost stable with annealing time at 1273 K (1000 °C) due to the little change of C and Mn content in austenite, as shown in
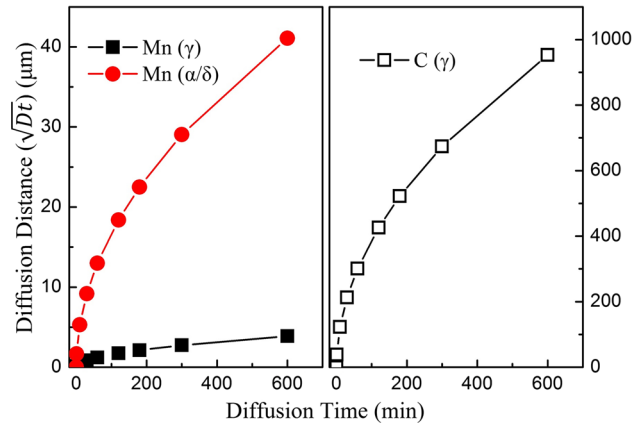

Fig. 13—Mean diffusion distance of C and Mn in different phases of the 10Mn steel at 1473 K (1000 °C).

Figure 11(a). Accordingly, the calculated martensite fraction without grain size effect only changes slightly (less than 2 vol pct), as observed in Figure 11(b). However by taking into account the austenite grain size, the M_s temperature shows a significant increase initially during the early 1 to 2 minutes and it stabilizes subsequently with annealing time. This reveals that the effect of grain size is dominant at early stages where the austenite grains are small, whereas this effect becomes almost negligible above certain sizes (here about 5 μm). The calculated martensite fraction accounting for grain size, as shown in Figure 11(b), exhibits a similar trend compared with the experimental data, although the calculated value is slightly higher; it first increases at the beginning and remains almost unchanged after certain amount of time.

IV. DISCUSSION

The observed results in "Section III" suggested that the final microstructure of the 7Mn steel depended substantially on the annealing temperatures. Higher

temperatures promote austenite formation but dilute the C and Mn contents and degrade the stability of the austenite which tends to transform to martensite upon quenching. The volume fraction of retained austenite could range from 0 to ~40 pct, and the martensite fraction was between 0 to ~25 vol pct, revealing a strong microstructural diversity, which was also reported by other researchers in medium Mn steels.[8,12,13,39] The mechanical property of the 7Mn steel was highly influenced by its microstructure. Micro-shear punch tests revealed that the FADP microstructure is superior to the FMNA microstructure in terms of both strength and ductility (the data can be found elsewhere[27]). In contrast, the 10Mn steel exhibited a FADP microstructure containing ~50 vol pct austenite which was found to be independent of the variations of intercritical annealing temperature. This noticeable stable ferrite-austenite duplex microstructure, to our knowledge, was never reported in medium Mn steels; similar structure could only be found in high alloyed steels, *e.g.*, duplex stainless steels[40] or a Fe-0.6C-20Mn-9Al steel reported by Hwang.[41] The mechanical properties for the 10Mn steel are also expected to be unaffected by annealing temperatures, as demonstrated in the previous work by shear punch tests.[27] Reported data for medium Mn steels indicated that the optimal combinations of strength and ductility can only be achieved in a very narrow annealing temperature range, *i.e.*, ~50 K.[1,7–9,16,42,43] Therefore, the processing robustness of the examined 10Mn steel constitutes an important advantage for its industrial production because a wide processing window exists in terms of optimum annealing temperature and subsequent cooling.

It has to be noted that upon reheating the δ-ferrite phase remains greater than 50 vol pct even at the highest annealing temperatures for both steels. This feature differs from the typical medium Mn TRIP steels that contain small amounts of Al and Si. For example, Han[44] investigated the effect of the heating rate on austenite formation in a 7 wt pct Mn steel with 0.3 wt pct Si and 0.1 wt pct Al, and found that the structure achieved 100 pct austenite at 1039 K (766 °C) for 3 K/s (°C/s) heating rate. Obviously, the addition of 3 wt pct Al and Si effectively stabilizes ferrite and enlarges the ferrite-austenite domain in the examined steels. This is also confirmed by Suh[25] who studied the effect of Al content on the microstructure of 5 wt pct Mn steels, and found that a single austenite phase domain disappeared as Al content exceeded beyond 3 wt pct. Although this stable δ-ferrite increases the complexity of the microstructure, it could bring about two benefits: (1) It promotes additional C and Mn partitioning between austenite and ferrite to further enrich the intercritical austenite (as shown in Figure 10), as such it enhances the stability of austenite. (2) It was reported by Lee[26] that localized deformation (Lüders bands propagation) could be suppressed by the coarse-grained δ-ferrite. However, the detailed effect of such a large amount of δ-ferrite on the mechanical properties of medium Mn steels is still unclear and requires further exploration in the future.

CALPHAD method is commonly used to preselect suitable heat treatment parameters in multicomponent systems. The austenite equilibrium fraction and composition at different temperatures were calculated using the commercial thermodynamic software, Thermo-Calc®, with both the commercial TCFE7 database and a modified thermodynamic database which was proposed by Hallstedt[45] initially for high Mn steels. The calculated austenite fractions from both databases, together with the experimental data, are shown in Figure 12. The two databases predict similar results for the 10Mn steel and the 7Mn steel at lower temperatures. However, the modified database achieves some improvement for the 7Mn steel at the higher temperature range (Figure 12 (a)), *e.g.*, a fully austenite domain should exist with the temperature above 1376 K (1103 °C) predicted by the TCFE7 database, whereas the modified database predicts a dual phase microstructure at this temperature range, matching the experimental observations. Nevertheless, the predicted austenite fractions in both alloys exhibit a large deviation from the measurements, although a similar trend with annealing temperature can be observed. The calculated austenite compositions of the two alloys from the modified database are also compared with the experimental measurements in Figure 7. The predicted austenite Al and Si contents agree very well with the experimental results. However, the calculated austenite Mn contents in both alloys have nearly 1 wt pct deviation from the experimental results. Further, it should be noted that in the 10Mn steel, the experimental austenite Mn content does not follow the trend of the prediction at low temperatures. The difference of the austenite C content between the calculation and the experimental data is even larger for both alloys. This discrepancy of the austenite C and Mn contents compared to the measured values stem from the overestimation of austenite volume fraction by the thermodynamic data. It has to be noted that the annealing time was insufficient to permit the alloying elements reaching their equilibrium partitioned state. However, as shown in Figure 10(a), C contents in austenite of both steels seem to be unchanged during annealing, indicating a constraint equilibrium is achieved rapidly. On the other hand, the Mn enrichment in austenite is very small (Figure 10(c)), so that prolonged annealing beyond 1 hour would not help to eliminate the discrepancy between the experimental and calculated Mn contents of the austenite. Further, the Mn contents in austenite keep increasing with time, which means the experimental austenite Mn contents will always exceed the prediction even with sufficient diffusion because most of the experimental data are already higher than the calculation after 1 hour annealing (Figure 7). This implies the deviation between the thermodynamic data and the experimental results would not be reduced even sufficient annealing time could be applied to reach equilibrium state. Therefore, this deviation could most likely to be derived from the inaccuracy of the thermodynamic database, which needs to be checked and further optimized for this type of medium Mn steels.

As mentioned in "Section III-C," austenite formation was very rapid at 1273 K (1000 °C) and the fraction of austenite remained invariably unchanged with annealing time in the examined medium Mn steels (Figure 9). However, it was proposed by Speich[46] and confirmed by other researchers[47–50] that austenite formation could be separated into three steps in dual-phase (DP) steels with ferrite-carbide mixtures: 1. austenite nucleation and carbon-diffusion-controlled growth of austenite following carbides dissolution; 2. further austenite growth into ferrite, controlled by Mn diffusion in ferrite in the intercritical temperature range; 3. final equilibration of ferrite and austenite controlled by sluggish Mn diffusion in austenite.

Generally, the first step is very rapid,[46,50,51] for example, it only took 0.12 ms in a 0.12C-1.5Mn steel at 1173 K (900 °C) and 50 ms in a 0.1C-3.4 Mn alloy at 1013 K (740 °C) calculated respectively by Speich[46] and Lai,[50] as such this stage normally cannot be observed experimentally. This is due to very high diffusivity of C atoms and the short diffusion distance (about equal to the interlamellar spacing of the pearlite[52] and the thickness of the thin bainite plate[53]). The traditional mean diffusion distance $(\sqrt{Dt})$ of C and Mn atoms in different phases of the 10Mn steel at 1273 K (1000 °C) was calculated and is shown in Figure 13, where D is the diffusion coefficient selected from the literatures[54–57] and t is the diffusion time. It shows that at this temperature, C diffuses almost 25 times faster than Mn in ferrite and 250 times faster than Mn in austenite. As shown in Figure 10(a), C content in austenite remains almost unchanged after 1 minute; on the other hand, the calculated value based on lever rule is quite close to the XRD measured value, indicating the carbides are completely dissolved after 1 minute. Therefore, in the present work, it is highly possible that the carbon-controlling step was completed before 1 minute or even during the course of heating. It should be noted that the austenite formation kinetics from pearlite and bainite would possess some difference depending on the carbide distribution, composition and morphology, but this difference could be in a very small magnitude which would be detected hardly by conventional experiments.

The second austenite formation step proposed by Speich is characterized by an intermediate slow growth of austenite (10^3 to 10^6 seconds[48]), followed by the third equilibration step which tends to be extremely slow.[46] Obviously, there was no direct evidence for additional growth of austenite during isothermal holding beyond one minute during annealing at 1273 K (1000 °C), as illustrated by Figure 9, namely the second austenite formation step is "absent." It can be argued that the second step which is controlled by Mn diffusion in ferrite is also very rapid and could be almost finished before 1 minute or during heating, as proposed in Lai's study.[50] This seems reasonable considering the relatively high annealing temperature selected in this work. However, the fraction of δ-ferrite is almost unchanged during annealing, for instance, the hot rolled 7Mn steel consists of 59.6 vol pct δ-ferrite, which is quite similar to the values after annealing (55 to 61 vol pct). This reveals

no tangible austenite growth into ferrite occurred, which was also confirmed by careful comparison of the microstructures before and after annealing in the same area.[27] Nevertheless it was found that Mn atoms had chance to redistribute slightly in the two phases after 1 minute, as shown in Figure 10 (c). Apparently two different kinetic regimes can be identified. First, Mn continued depleting in ferrite while almost invariant in austenite, which could correspond to the step 2 proposed by Speich.[46] Second, at longer holding time, Mn content of ferrite remained almost constant while ramped up in austenite, corresponding to the final equilibration stage (stage 3) in Speich and other researchers' work.[46–50] This observation implied that the Mn redistribution in ferrite actually could occur and most likely complete before the final equilibration stage. However, due to very slight amount of redistribution (<0.5 wt pct) which is controlled by the probably small ferrite to austenite transformation driving force, a tangible change in austenite fraction could not be detected experimentally. In terms of processing implication, the results suggest that a long annealing time is irrelevant for these steels and a short annealing time, in the order of a few minutes, is adequate; showing another advantage of these medium Mn grades to enhance production rate and energy saving.

V. CONCLUSIONS

The microstructural evolution of two high Al-Si medium Mn (7 and 10 wt pct) hot rolled steels upon intercritical annealing and subsequent quenching to room temperature were investigated. The following conclusions can be summarized:

1. The annealing temperature had a substantial influence on the microstructure of the 7Mn steel, including the variation of phase constituents, austenite morphology and composition (mainly C and Mn content), the M_s temperature and retained austenite fraction. The fraction of retained austenite peaked at ~40 vol pct for intercritical treatment at 1173 K (900 °C). However, the 10Mn steel was not sensitive to the annealing temperature, showing an invariant ferrite-austenite duplex microstructure with ~50 vol pct austenite regardless of the annealing temperature. The Mn content of austenite in the 10Mn steel also remained nearly unchanged at different annealing temperatures; this higher Mn value enhanced the austenite stability and maintained the M_s temperature below ambient temperature. Both steels possessed a large fraction of δ-ferrite (higher than 50 vol pct) before heat treatments, which was stabilized by Al and Si and maintained intact during intercritical annealing.

2. Transformation of initial ferrite-pearlite/bainite hot band microstructure into austenite is very rapid upon heating and additional isothermal holding in both steels. Austenite growth is believed to be first controlled by C diffusion in austenite following pearlite/bainite dissolution. Subsequently, Mn atoms

tend to redistribute first in ferrite and at later stages in austenite. However, the amount of Mn partitioning and redistribution was too subtle (less than 0.5 wt pct) to result in a tangible change in austenite fraction for the examined annealing time.

3. A modified thermodynamic database was evaluated using the experimental data. Although the new database achieved a better agreement with the experimental results for the 7Mn steel compared with TCFE7, some discrepancy in the predicted phase fractions and compositions over a range of intercritical temperatures still existed for the examined steels. The experimental results in the present work could be exploited to optimize the existing thermodynamic database for such high Al-Si medium Mn steels.

REFERENCES

1. N. Fonstein: *Advanced High Strength Sheet Steels: Physical Metallurgy, Design, Processing, and Properties*, Springer, Switzerland, 2015, vol. 2015, pp. 297–323.
2. Y.K. Lee and J. Han: *Mater. Sci. Technol.*, 2015, vol. 31, pp. 843–56.
3. O. Bouaziz, H. Zurob, and M. Huang: *Steel Res. Int.*, 2013, vol. 84, pp. 937–47.
4. R.L. Miller: *Metall. Trans.*, 1972, vol. 3, pp. 905–12.
5. H. Aydin, E. Essadiqi, I.H. Jung, and S. Yue: *Mater. Sci. Eng. A*, 2013, vol. 564, pp. 501–08.
6. A. Arlazarov, M. Gouné, O. Bouaziz, A. Hazotte, G. Petitgand, and P. Barges: *Mater. Sci. Eng. A*, 2012, vol. 542, pp. 31–39.
7. P.J. Gibbs, E. De Moor, M.J. Merwin, B. Clausen, J.G. Speer, and D.K. Matlock: *Metall. Mater. Trans. A*, 2011, vol. 42A, pp. 3691–3702.
8. S. Lee and B.C. De Cooman: *Metall. Mater. Trans. A*, 2013, vol. 44A, pp. 5018–24.
9. S. Lee, S.J. Lee, S.S. Kumar, K. Lee, and B.C. De Cooman: *Metall. Mater. Trans. A*, 2011, vol. 42A, pp. 3638–51.
10. W. Cao, C. Wang, J. Shi, M. Wang, W. Hui, and H. Dong: *Mater. Sci. Eng. A*, 2011, vol. 528A, pp. 6661–66.
11. H. Huang, O. Matsumura, and T. Furukawa: *Mater. Sci. Technol.*, 1994, vol. 10, pp. 621–26.
12. E. De Moor, D.K. Matlock, J.G. Speer, and M.J. Merwin: *Scripta Mater.*, 2011, vol. 64, pp. 185–88.
13. P.J. Gibbs: *Design Considerations for the Third Generation Advanced High Strength Steel*, Metallurgical and Materials Engineering, Colorado School of Mines, Golden, 2012, pp. 1–79.
14. S. Lee, S.J. Lee, and B.C. De Cooman: *Scripta Mater.*, 2011, vol. 65, pp. 225–28.
15. S. Lee and B.C. De Cooman: *Steel Res. Int.*, 2015, vol. 86, pp. 1–9.
16. S. Lee and B.C. De Cooman: *Metall. Mater. Trans. A*, 2014, vol. 45A, pp. 6039–52.
17. B. Sun, H. Aydin, F. Fazeli, and S. Yue: *Metall. Mater. Trans. A*, 2016, vol. 47A, pp. 1782–91.
18. S.S. Sohn, K. Choi, J.H. Kwak, N.J. Kim, and S. Lee: *Acta Mater.*, 2014, vol. 78, pp. 181–89.
19. C.Y. Lee, J. Jeong, J. Han, S.J. Lee, S. Lee, and Y.K. Lee: *Acta Mater.*, 2015, vol. 84, pp. 1–8.
20. S. Lee, K. Lee, and B.C. De Cooman: *Metall. Mater. Trans. A*, 2015, vol. 46, pp. 2356–63.
21. H. Kim, D.W. Suh, and N.J. Kim: *Sci. Technol. Adv. Mater.*, 2013, vol. 14, pp. 1–11.
22. H. Aydin, I.H. Jung, E. Essadiqi, and S. Yue: *Mater. Sci. Eng. A*, 2014, vol. 591, pp. 90–96.
23. K. Jeong, J.E. Jin, Y.S. Jung, S. Kang, and Y.K. Lee: *Acta Mater.*, 2013, vol. 61, pp. 3399–3410.
24. B.W. Oh, S.J. Cho, Y.G. Kim, Y.P. Kim, W.S. Kim, and S.H. Hong: *Mater. Sci. Eng. A*, 1995, vol. 197, pp. 147–56.
25. D.W. Suh, S.J. Park, T.H. Lee, C.S. Oh, and S.J. Kim: *Metall. Mater. Trans. A*, 2010, vol. 41A, pp. 397–408.
26. S. Lee, Y. Estrin, and B.C. De Cooman: *Metall. Mater. Trans. A*, 2013, vol. 44A, pp. 3136–46.
27. B. Sun, H. Aydin, F. Fazeli and S. Yue: *MS and T 2015 Conf. Proc.*, Columbus, United States, 2015, pp. 893–900.
28. R.A. Young: *The Rietveld Method*, International Union of Crystallograhy, Oxford, New York, 1995.
29. ASTM Standard E1245 - 03: *Standard Practice for Determining the Inclusion or Second-Phase Constituent Content of Metals by Automatic Image Analysis*, ASTM International, West Conshohocken, PA, 2012. www.astm.org.
30. ASTM Standard E112 - 12: *Standard Test Methods for Determining Average Grain Size*, ASTM International, West Conshohocken, PA, 2012. www.astm.org.
31. N.H. van Dijk, A.M. Butt, L. Zhao, J. Sietsma, S.E. Offerman, J.P. Wright, J.P. Wright, and S. Van der Zwaag: *Acta Mater.*, 2005, vol. 53, pp. 5439–47.
32. D.J. Dyson and B. Holmes: *J. Iron Steel Inst.*, 1970, vol. 208, pp. 469–74.
33. B.D. Cullity: *Elements of X-ray Diffraction*, Addison-Wesley Pub. Co, Cambridge, 1978, vol. 2, p. 459.
34. M. Calcagnotto, D. Ponge, E. Demir, and D. Raabe: *Mater. Sci. Eng. A*, 2010, vol. 527, pp. 2738–46.
35. S.J. Lee, S. Lee, and B.C. De Cooman: *Int. J. Mater. Res.*, 2013, vol. 104, pp. 423–29.
36. D.P. Koistinen and R.E. Marburger: *Acta Metall.*, 1959, vol. 7, pp. 59–60.
37. S.J. Lee and C.J. Van Tyne: *Metall. Mater. Trans. A*, 2012, vol. 43A, pp. 422–27.
38. S.J. Lee, S. Lee, and B.C. De Cooman: *Scripta Mater.*, 2011, vol. 64, pp. 649–52.
39. M. Cai, Z. Li, Q. Chao, and P.D. Hodgson: *Metall. Mater. Trans. A*, 2014, vol. 45A, pp. 5624–34.
40. International Molybdenum Association (IMOA): *Practical guidelines for the fabrication of duplex stainless steels*, International Molybdenum Association (IMOA), London, U.K., 2009, vol. 2, pp. 10–13.
41. S.W. Hwanga, J.H. Jib, E.G. Leeb, and K.T. Park: *Mater. Sci. Eng. A*, 2011, vol. 528, pp. 5196–203.
42. D.W. Suh, J.H. Ryu, M.S. Joo, H.S. Yang, K. Lee, and H.K.D.H. Bhadeshia: *Metall. Mater. Trans. A*, 2013, vol. 44A, pp. 286–93.
43. T. Furukawa: *Mater. Sci. Technol.*, 1989, vol. 5, pp. 465–70.
44. J. Han and Y.K. Lee: *Acta Mater.*, 2014, vol. 67, pp. 354–61.
45. B. Hallstedt, A.V. Khvan, B.B. Lindahl, and M. Selleby: *CALPHAD XLIV*, Loano, Italy, 2015, unpublished research.
46. G.R. Speich, V.A. Demarest, and R.L. Miller: *Metall. Trans. A*, 1981, vol. 12, pp. 1419–28.
47. X.L. Cai, A.J. Garratt-Reed, and W.S. Owen: *Metall. Trans. A*, 1985, vol. 16, pp. 543–57.
48. J. Ågren: *Acta Metall.*, 1982, vol. 30, pp. 841–51.
49. A. Arlazarov: *Evolution of Microstructure and Mechanical Properties of Medium Mn Steels and Their Relationship*, University of Lorraine, France, 2015, pp. 109–17.
50. Q. Lai: *Optimization of the Microstructure of Ferritic-Martensitic Steels with 3.5 wt. % Mn: Phase Transformations and Micromechanical Modeling*, Joseph Fourier University, France, 2014, pp. 44–64.
51. M. Gouné, P. Maugis, and J. Drillet: *J. Mater. Sci. Technol.*, 2012, vol. 28, pp. 728–36.

52. G.R. Speich, A. Szirmae, and M.J. Richards: *Trans. TMS-AIME*, 1969, vol. 245, pp. 1063–74.
53. J.R. Yang and H.K.D.H. Bhadeshia: *Mater. Sci. Eng. A*, 1989, vol. 118, pp. 155–70.
54. C. Wells and R.F. Mehl: *Trans. Am. Inst. Min. Met. Pet. Eng.*, 1941, vol. 145, pp. 315–28.
55. J. Ågren: *Scripta Metall.*, 1986, vol. 20, pp. 1507–10.
56. G Neumann and C Tuijn: *Self-diffusion and Impurity Diffusion in Pure Metals: Handbook of Experimental Data*, 1st ed., Elsevier Ltd., Oxford, 2009, pp. 261–74.
57. J.S. Kirkaldy, P.N. Smith, and R.C. Sharma: *Metall. Trans. B*, 1973, vol. 4, pp. 624–25.